
Article:
Chen, C., Farrer, I., Holmes, S.N. et al. (2015) Growth variations and scattering mechanisms in metamorphic In0.75Ga0.25As/In-0.75 Al0.25As quantum wells grown by molecular beam epitaxy. Journal of Crystal Growth, 425. 70 - 75. ISSN: 1062-7995

https://doi.org/10.1016/j.jcrysgro.2015.02.038

Growth Variations and Scattering Mechanisms in Metamorphic $In_{0.75}Ga_{0.25}As/In_{0.75}Al_{0.25}As$ Quantum Wells Grown by Molecular Beam Epitaxy

Chong Chen[a,*], Ian Farrer[a], Stuart N. Holmes[b], Francois Sfigakis[a], Marc P. Fletcher[a], Harvey E. Beere[a], David A. Ritchie[a]

[a] *Cavendish Laboratory, University of Cambridge, JJ Thomson Avenue, Cambridge CB3 0HE, United Kingdom*
[b] *Toshiba Research Europe Limited, Cambridge Research Laboratary, 208 Cambridge Science Park, Milton Road, Cambridge CB4 0GZ, United Kingdom*

Abstract

Modulation doped metamorphic $In_{0.75}Ga_{0.25}As/In_{0.75}Al_{0.25}As$ quantum wells (QW) were grown on GaAs substrates by molecular beam epitaxy (MBE) with step-graded buffer layers. The electron mobility of the QWs has been improved by varying the MBE growth conditions, including substrate temperature, arsenic over pressure and modulation doping level. By applying a bias voltage to SiO_2 insulated gates, the electron density in the QW can be tuned from 1×10^{11} to 5.3×10^{11} cm^{-2}. A peak mobility of 4.3×10^5 cm^{2}V^{-1}s^{-1} is obtained at 3.7×10^{11} cm^{-2} at 1.5 K before the on-set of second subband population. To understand the evolution of mobility, transport data is fitted to a model that takes into account scattering from background impurities, modulation doping, alloy disorder and interface roughness. According to the fits, scattering from background impurities is dominant while that from alloy disorder becomes more significant at high carrier density.

Keywords: $In_{0.75}Ga_{0.25}As$, Quantum Well, Molecular Beam Epitaxy, Atomic Force Microscope, Electron transport, Scattering Mechanisms,

2010 MSC: 00-01, 99-00

*Corresponding author
Email address: cc638@cam.ac.uk (Chong Chen)

1. Introduction

$In_xGa_{1-x}As/In_xAl_{1-x}As$ quantum wells (QWs) are attractive because of the low electron effective mass, large g-factor, large Rashba spin-orbit coupling and highly transmissive metal-semiconductor interface at high indium composition compared to GaAs/AlGaAs [1]. It also provides a way of varying these parameters by changing the composition of the indium.

However, when compared with its couterpart GaAs/AlGaAs, there is a fundamental issue regarding growth. There is no lattice matched substrate for growing InGaAs except for $In_{0.53}Ga_{0.47}As/In_{0.52}Al_{0.48}As$ on InP. Researchers have incorporated graded InGaAs or InAlAs layer to grow high percentage InGaAs on InP or GaAs [2, 3, 4] and managed to achieve control of propagation of dislocations due to strain [2, 4, 5, 6]. Virtually strain-free, defect-free layers can be achieved through the use of step-graded buffer layers with compositional "overshoot" [5]. An electron mobility of 2.9×10^5 $cm^2V^{-1}s^{-1}$ was obtained at 4.0×10^{11} cm^{-2} [5].

Scattering mechanisms in relaxed and strained InGaAs/InAlAs quantum wells have been studied by several researchers [1, 2, 7]. Their research has shown that scattering from background impurities limits the mobility at lower carrier densities, scattering from alloy disorder becomes more important at higher carrier densities. Capotondi et al. [1] reduced the impact of alloy disorder by inserting binary InAs into the quantum well. Understanding how each scattering mechanism influences the total mobility is crucial when attempting to further improve mobility in InGaAs which could make the realisation of spin and/or Josephson FETs possible [8, 9].

In this paper, we present a transport study on a series of wafers grown under different conditions with nominally the same layer strucuture to investigate the difference in mobility. AFM (Atomic Force Microscope) images of the free surface are used to provide supplementary information of the surface or interface morphology. The transport measurements were performed at 1.5 K. The mobility fits were using the theory provided by A. Gold [10]. This work aims to

understand the influence of different scattering mechanisms and therefore, make possible suggestions for further improvements to the layer structure or growth conditions.

2. Experiment

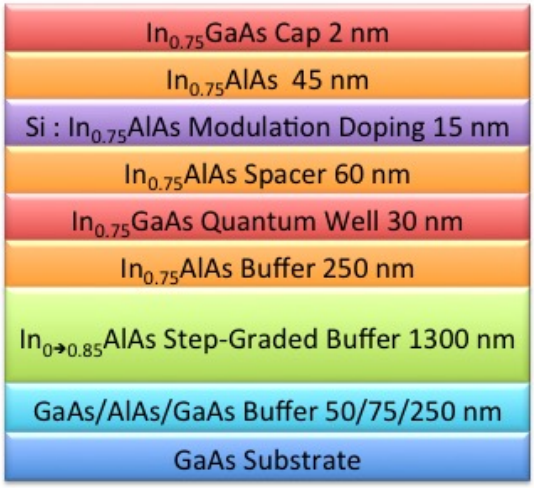

Figure 1: Schematic layer structure of $In_{0.75}Ga_{0.25}As/In_{0.75}Al_{0.25}As$ Quantum Wells

The quantum wells studied in this paper were grown by solid-source molecular beam epitaxy (MBE) using a Veeco Gen III system on 3 inch semi-insulating (001) GaAs substrates that are indium-free mounted. A schematic layer structure adapted from [5, 11, 12] is shown in Fig. 1. Arsenic dimers (As_2) rather than arsenic tetramers (As_4) are used to try and reduce antisite defects at the low growth temperatures used (330-420°C) [13]. Three growth parameters, substrate temperature (T_B), arsenic over pressure (P_{As_2}) and Si modulation doping level (N_{Si}) were adjusted to improve the electron mobility in this structure. T_B was measured using a kSA BandiT system [14] and where possible also with an

optical pyrometer. T_B was set at the start of the graded buffer layer growth and not intentionally further altered during the growth. Growth temperatures quoted throughout this work refer to those measured by BandiT unless specified.

After oxide removal and degassing, the GaAs/AlAs/GaAs buffer was grown at 580°C. Then the substrate temperature is ramped down over a period of 20 minutes before growing the step-graded buffer (SGB) layer. The step-graded buffer layer was grown at six different starting substrate temperatures: 416°C, 390°C, 360°C, 341°C, 331°C and 337°C. The first growth temperature was chosen according to Simmonds' study [12] where the growth temperature for devices grown on InP substrates was optimised. The quantum wells are grown at slightly higher substrate temperatures as the substrate becomes more absorbing during growth. To alter the indium composition in the structure, the aluminium cell temperature is ramped down while the indium cell temperature is ramped up rapidly at the start of each layer in the SGB sequence. To change the arsenic over pressure, the needle valve in the arsenic cell was adjusted and the pressure is measured by the beam flux gauge prior to growth. The nominal growth rate is kept the same (around 1.0 μm/h) throughout the structure. Growth was interrupted to stablise the In cell to grow the 75% InAlAs buffer. This interruption introduces the possiblity of impurity accumulation [12], therefore a further 250 nm InAlAs layer is grown afterwards to separate the impurities from the conduction channel. The first sample was grown undoped to replicate the growth condition in [12], however it did not conduct without illumination at 1.5 K. The remaining 5 wafers were then modulation doped to ensure conductance in the dark. The modulation doping concentration is controlled by altering the Si cell temperature. The major differences in growth conditions are highlighted in Table 1.

The AFM images are taken with a Veeco Dimension 3000 SPM (Scanning Probe Microscope) and Nanoworld pointprobe. The size of the scanned area is 10×10 μm^2 which is large enough to be representative of the surface morphology. High Electron Mobility Transistors (HEMTs) were fabricated using standard wet chemical etching. AuGeNi alloy was used for Ohmic contacts, PECVD

Table 1: Growth detail

Wafer No.	W0401	W0402	W0413	W0414	W0435	W0436
T_B (°C)	416	391	360	341	331	337
T_P (°C)	470	462	437	431	428	429
P_{As_2} ($\times 10^{-5}$ torr)	1.2	1.2	1.4	1.4	1.2	1.0
N_{Si} ($\times 10^{17} cm^{-3}$)	0	2.3	2.3	2.3	1.8	1.8

T_B/T_P: Substrate temperature measured by BandiT/Pyrometer at the start of SGB/QW growth; P_{As_2}: As_2 Beam Flux; N_{Si}: Si Modulation Doping Level.

Silicon dioxide (100 nm) for insulator and thin NiCr (20 nm) for transparent gate. The chips were taken from the same position on each wafer. Shubnikov-de Haas oscillations and Hall effect are measured at 1.5 K to obtain electron density and mobility.

3. Result and discusstion

3.1. AFM

The morphology of the free surface is studied as an indirect reference to the buried $In_{0.75}Al_{0.25}As/In_{0.75}Ga_{0.25}As$ interface, since we assume that the lattice is fully relaxed according to [11] and the surface undulation result from the misfit dislocation network buried in the buffer layer[5]. The digitization lateral step size of the following images is 20 nm.

As seen in Fig. 2, the surface grown at the highest temperature Fig. 2a has the roughest morphology with long 3D islands due to the tensile strain during crystal growth[15]. When the temperature is decreased from 416°C to 390°C the size of the islands reduces, with further decrease of the growth temperature, the islands become less visible but more aligned. The surface begins to show the well-known cross-hatched pattern. A change from 3D growth mode (2a and 2b) to 2D growth mode (2c, 2d, 2e and 2f) and a corresponding reduction, by

a factor of 3, of the RMS value can be seen when the growth temperature is decreased. This is because the surface diffusion length is reduced and therefore the layer-by-layer growth regime is extended[15].

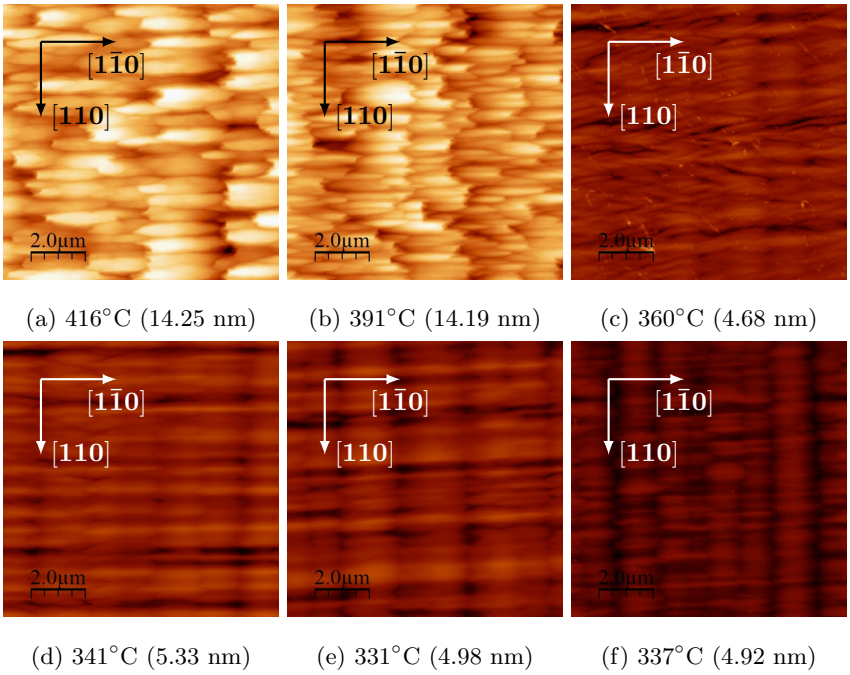

(a) 416°C (14.25 nm) (b) 391°C (14.19 nm) (c) 360°C (4.68 nm)

(d) 341°C (5.33 nm) (e) 331°C (4.98 nm) (f) 337°C (4.92 nm)

Figure 2: $10\times10\ \mu m^2$ AFM images show significant improvement in surface morphology when decreasing the growth temperature. The z-axis scale is adjusted to be 100 nm in each image for comparison. The Root mean square (RMS) roughness value, given in the subcaption, is averaged from 5 images taken from different positions on the wafer.

The surface morphology is clearly anisotropic. The islands seen in 2a and 2b are elongated along [1$\bar{1}$0]. There are striations aligned to [1$\bar{1}$0] in other samples. The period of surface oscillation appeares to be crystallographic direction dependent. This difference in surface undulation was also observed previously [5, 16, 17].

3.2. Transport

Figure 3 shows the electron mobility (μ) as a function of electron density (n_{2d}) for $In_{0.75}GaAs$ quantum wells. Electron density was varied by applying a gate voltage from the beginning of 2DEG depletion to the saturation of electron density. In reference [12], the growth at 410°C showed the highest mobility. In the present set of wafers, sample grown at a similar temperature (W0401 at 416°C) did not conduct without illumination. The mobility of W0401(416°C) is only comparable with the crystal grown at 470°C (Fig.3 in [12]) but with slightly higher carrier densities. Extra carriers in W0401 could come from modulation dopants and unintentional dopants from the thicker buffer layer compared with InGaAs QWs grown on InP substrate [12]. The growth temperature at the quantum well region in W0401 is 470°C which is a comparable growth temperature in [12]. Therefore, the two samples have similar mobility although based on different substrates.

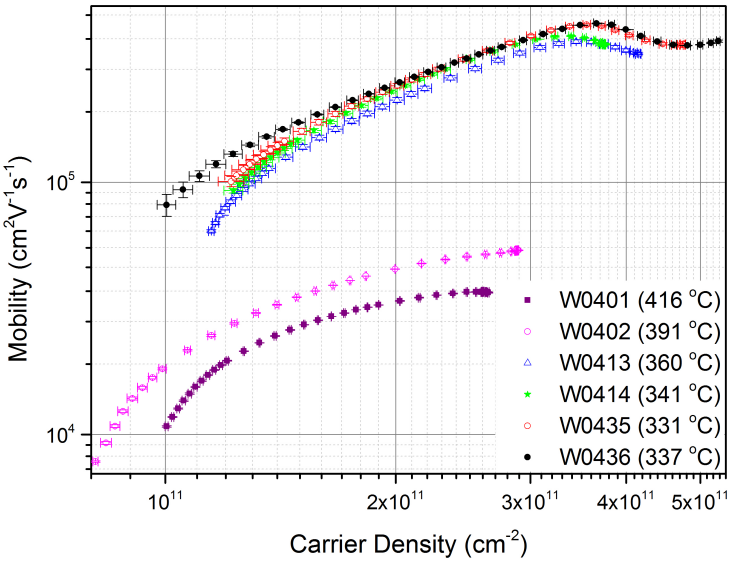

Figure 3: Electron mobility as a function of electron density at 1.5 K.

The fact that the surface morphology of sample W0401 is rough and does not conduct in the dark indicates that it has been grown at a too high tempera-

ture. In order to improve the surface morphology, the growth temperature was lowered to 391°C when growing the next sample W0402. Modulation doping was implemented to make the sample conduct in the dark. As shown in Fig. 2 and 3, the surface morphology and the mobility of W0402 improved comparing with W0401, but it is not comparable with that presented in [1]. The growth temperature was further reduced to 360°C and arsenic over pressure was increased in W0413 which lead to significant improvements in both morphology and mobility. Although a further reduction in growth temperature in W0414 (341°C) did not improve surface morphology, it did improve the mobility. High arsenic over pressure would improve the surface morphology, however, it may introduce more background impurities. Steps to improve the mobility was then made by controlling the scattering from ionised impurities, reducing the arsenic over pressure and the modulation doping level as for W0435 while keeping the growth temperature at roughly the same level (10°C lower at the start of SGB and 3°C lower at the beginning of QW). The arsenic over pressure was further reduced in W0436 while maintaining the growth temperature. The mobility of W0435 and W0436 is similar over whole density range except W0436 shows a slightly higher peak mobility around 4.3×10^5 cm^{2}V^{-1}s^{-1} at 3.7×10^{11} cm^{-2}. Transport data from W0436 will be discussed more detailly in the following sections.

In all wafers, the μ increases monotonically with n_{2d} to its peak value; a decrease is seen in mobility above a critical density (n_c) in the four wafers the density of which reaches $3.4\times10^{11}cm^{-2}$. This decrease was also observed by Capatondi in their undoped relaxed structures [1] and Ramvall in their strained structures [7]; however, only two of the best mobility structures showed an increase in mobility after the minimum mobility. This feature, due to the second-subband population, is confirmed by multiple frequencies in the Shubnikov-de Haas oscillation as shown in Fig 4. Fast Fourier transform performed at different carrier densities demonstrates the evolution of the second subband. The electron density in the first subband (F1 in 4) is constant while that inside the second subband increases as the total density increases. No clear beating effect is

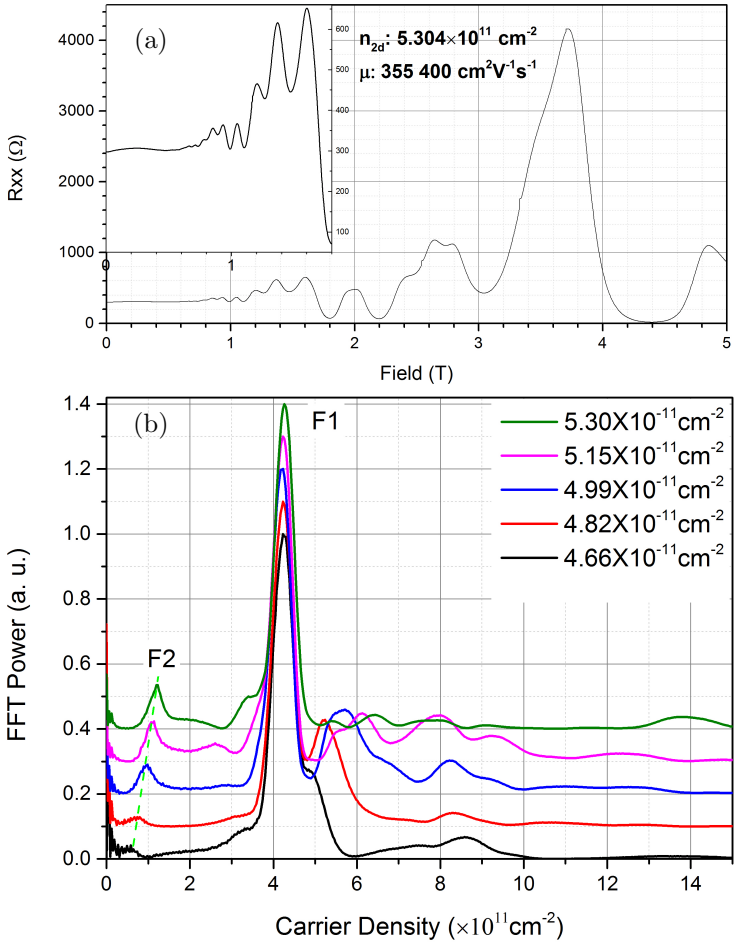

Figure 4: (a) A representative longinitudial resistance measurement on W0436 shows multiple frequncies in the Shubnikov-de Haas oscillations; the inset shows the low field region in more detail; (b) Fast Fourier Transform results from Shubnikov-de Haas oscillations at different densities by changing the gate voltage in enhancement mode (F1 and F2 are the first and second subband). The legends are carrier densities obtained from the Hall measurement slopes which agree well with densities calculated from FFT.

observed in the Shubnikov-de Haas effect nor spin-split in FFT. Therefore, the multiple frequencies in Shubnikov-de Haas effect is not due to Rashba effect but due to the second subband population [18].

Using a magnetic field modulation technique[19], the Rashba coefficient (α) was measured to be $0.7\pm0.1\times10^{-11}$ eV·m in W0436 where peak splittings in the FFTs can be quantified. This corresponds to an energy splitting of 1.6 meV at the Fermi energy. The detailed measurement is not included in this work. The asysmmetry of the confining potential in the doped wafer does not enhance the Rashba coefficient compared to the nominally undoped wafers grown on InP in the authors' previous work[19]. Although modulation doping changes quite dramatically the symmetry of the confining potential, the spin-splitting in a quantum well system is mainly determined by the band offsets with the barrier material, not the electric field in the z-direction[20].

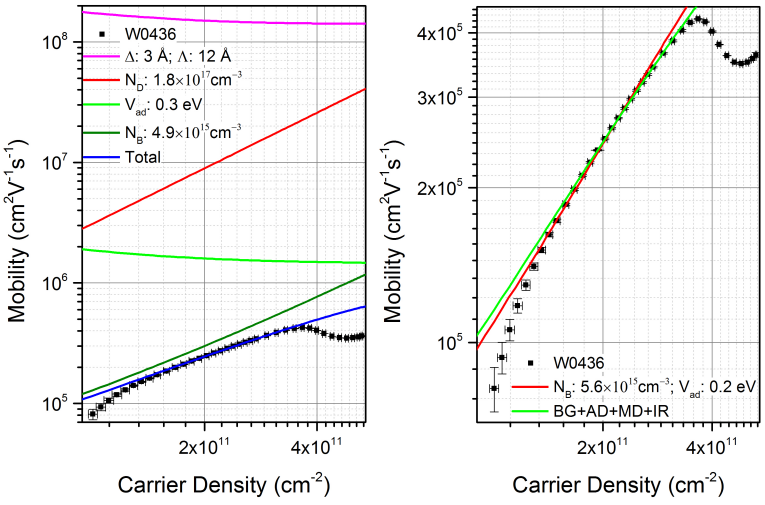

Figure 5: Left: Fitting example of taking Interface Roughness (IR: Δ, Λ), Modulation Doping (MD: N_D), Alloy Disorder (AD: V_{ad}), and Background Impurity (BG: N_B) scattering into consideration; right: comparison of two fittings: one with four scattering mechanisms ($R^2 = 0.9573$) and the other with only two of them (BG and AD, $R^2 = 0.8386$).

There are three main scattering mechanisms operating in these structures: ionised impurity scattering, alloy disorder scattering (AD), and interface roughness scattering (IR) [21]. The ionised impurity scattering can come from the background impurities (BG) or the modulation doping (MD). An example fit is shown in Figure 5(Left). There are some reports about charged dislocations acting as scattering centres [6, 16], however the mobility in these samples is only 50000 $cm^2V^{-1}s^{-1}$ at 3.6 $\times 10^{11}$ cm^{-2}. Consequently, scattering from charged dislocations is not considered in this paper since a study on a similar structure has demonstrated a defect-free conducting layer and the mobility in this work is comparable with that of [1].

Table 2: Fitting Parameters only considering background impurities and alloy disorder

Wafer No.	Background Impurity Level N_B (cm^{-3})	Alloy Disorder Potential V_{ad}(eV)
W0401(416°C)	3.7×10^{16}	0.2
W0402(391°C)	2.9×10^{16}	0.2
W0413(360°C)	6.5×10^{15}	0.2
W0414(341°C)	5.8×10^{15}	0.2
W0435(331°C)	$>5.6\times10^{15}$	0.2
W0436(337°C)	$<5.6\times10^{15}$	0.2

Single scattering mechanism fitting is done first to extract the reasonable range of the parameters, the background impurity level N_B, the activated dopants level N_D, the alloy disorder potentianl V_{ad}, the interface correlation length Λ and the average height of the surface Δ. V_{ad} will be the same for each wafer since the alloy composition is identical among them. We assume that the dopant activation rate is the same across this set of wafers. According to [22], we assume that at the doping level in this paper, Si is fully activated which means the activation rate is around 1. Scattering from MD is not the limiting

scattering mechanism since the mobility limited by MD is one magnitude larger (see Fig. 5). Therefore to simplify the fitting procedure the data using only BG and AD was carried out according to [1]. The extracted parameters are summarised in Table 2. By assuming the scattering from interface roughness is not significant, background impurity levels extracted from the fitting is very sensitive to changes in growth temperature and arsenic over pressure. One example fit is shown in Fig 5(right). As a comparison, the fitting that considers all four scattering mechanisms is presented in the same diagram. R-squared value has been calculated from 1.7×10^{11} cm^{-2} to 3.8×10^{11} cm^{-2} for these two fittings, the value from the four-mechanism fitting is 0.9573 and that from the two-mechanism fiting is 0.8386, therefore the four-mechanism fitting is more representative of the experimental data. Consequently, even though scattering from IR is not dominant, it is a significant contribution to the total mobility.

Table 3: Fitting parameters used in Figure 6

Wafer No.	MD	BG	AD	IR	
	N_d (cm^{-3})	N_B (cm^{-3})	V_{ad} (eV)	Λ (Å)	Δ (Å)
W0413(360°C)	2.3×10^{17}	5.5×10^{15}	0.3	300	6
W0414(341°C)	2.3×10^{17}	4.8×10^{15}	0.3	300	6
W0435(331°C)	1.8×10^{17}	4.5×10^{15}	0.3	100	3
W0436(337°C)	1.8×10^{17}	4.9×10^{15}	0.3	12	3

MD: Modulation Doping; BG: Background Impurities; AD: Alloy Disorder; IR: Interface Roughness.

The four-mechanism fitting is applied to the four high density wafers. The results are shown in Fig. 6 and the parameters used are listed in Table 3. The average height is chosen to be a multiple of the thickness of one monolayer. To be noted, the parameters for interface roughness is not taken from the AFM information. Since the lateral resolution of AFM is limited by both digitization

step size and the tip size which are 20 nm and 10 nm in this study, respectively. This is 2 orders larger than the lattice constant of InGaAs. A good fit can be made to each set of data by adjusting the background impurity level and the interface roughness. The extracted alloy disorder potential is 0.3 eV which agrees with the result, around 0.3 eV, reported by [7] for $In_{0.75}Ga_{0.25}As$ however smaller than the value (0.5 eV) reported by [5]. The extracted background impurity level is of the order of 10^{15} cm^{-3}. The fitted data agrees well with the experimental data from around $1\times10^{11}cm^{-2}$ to the point where the second subband populates. At the low density end where neither fitting method applies, the mobility is dominated by percolation which can only be fitted using metal-insulator transition theory[23]. At the high density end where second-subband populates (see Fig. 4), the mobility is limited by inter-subband scattering. The scattering from background impurities is dominating the whole density range, while alloy disorder scattering becomes increasingly important as the carrier density increases. To extract more accurate growth parameters, a further study has to be carried out to verify the assumptions made in this work, eg. relaxation of the crystal during growth.

It is interesting to see that all these wafers show anisotropy in mobility. The measured mobility difference in both direction on W0436 is shown in Fig. 7. This had been observed by many researchers [24, 17, 7]. This could result from a number of reasons such as interface roughness, indium concentration modulation or anisotropic ordering appeared in the structures. In this work, the mobility anisotropy appeares to follow the surface morphology anisotropy: the higher mobility is along $[1\bar{1}0]$ which has bigger undulation period. To verify the factors that account for this phenomena, a more detailed study is required.

4. Conclusion

The growth conditions for modulation doped $In_{0.75}Ga_{0.25}As/In_{0.75}Al_{0.25}As$ quantum wells on GaAs were studied. A sample grown under 1.0×10^{-5} torr

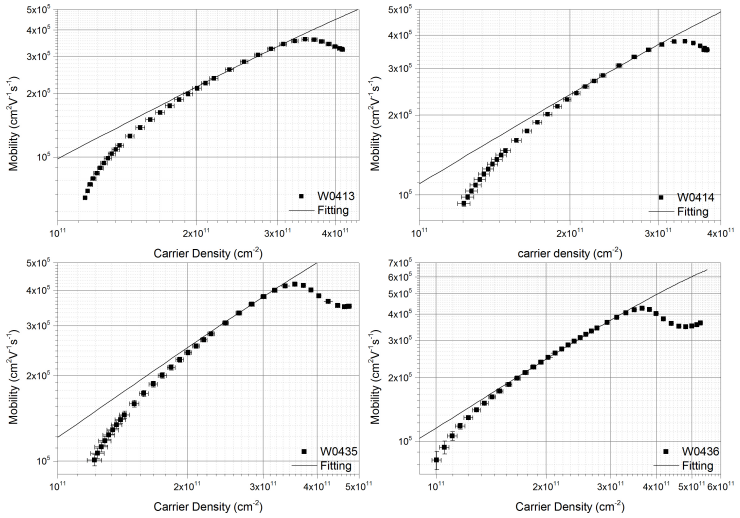

Figure 6: Four mechanisms fitting of all four wafers, the fitting parameters are listed in Table 3. The straight line is a fit to the data.

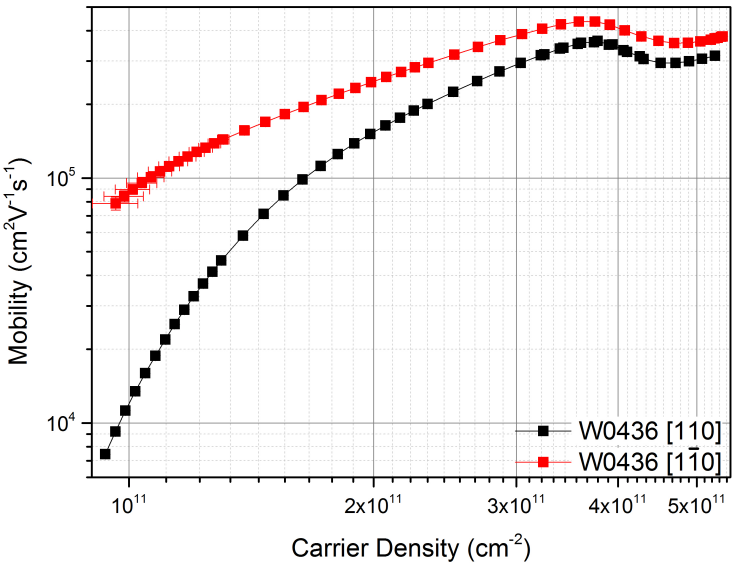

Figure 7: Anisotropy of mobility in two different crystallographic directions at 1.5 K which is present at all gate voltages.

arsenic over pressure with 1.8×10^{17} cm^{-3} modulation doping at 337°C has the highest mobility. A peak mobility of 4.3×10^{5} cm^{2}V^{-1}s^{-1} is obtained at 3.7×10^{11} cm^{-2} at 1.5 K with a gated structure. The SiO_2 insulated gates provides high reproducibility and low hysteresis from depletion to $\simeq5\times10^{11}$ cm^{-2}. We have demonstrated a promising fit to experimetal data using Gold's model considering four different scattering mechanisms, background impurities, modulation doping, alloy disorder and interface roughness scattering. We estimate the alloy disorder potential to be around 0.3 eV and the background impurity level of the order of $\sim10^{15}$ cm^{-3}. This could be used as a method to extract growth parameters[23] if the growth conditions or the layered structure is designed in a systematic way. Anisotropy in surface morphology and mobility is observed in all wafers. The Rashba coefficient calculated in these structures is similar to that in undoped structures. Although modulation doping enhances the asysmmetry across the quantum well, the Rashba coefficient is insensitive to this confirming the theory presented in [20].

References

[1] F. Capotondi, G. Biasiol, D. Ercolani, L. Sorba, Scattering mechanisms in undoped $In_{0.75}Ga_{0.25}As/In_{0.75}Al_{0.25}As$ two-dimensional electron gases, Journal of Crystal Growth 278 (1-4) (2005) 538–543.

[2] S. Gozu, T. Kita, T. Kikutani, S. Yamada, Critical layer thickness study in $In_{0.75}Ga_{0.25}As/In_{0.5}Al_{0.5}As$ pseudomorphic resonant tunneling diode structure grown on GaAs substrates, Journal of Crystal Growth 227-228 (2001) 161–166.

[3] M. Bergh, E. Olsson, T. G. Andersson, H. Zirath, Molecular beam epitaxy growth and characterization of $In_xGa_{1-x}As$ ($0.57 < x < 1$) on GaAs using InAlAs graded buffer, Journal of Crystal Growth 175/176 (1997) 1016–1021.

[4] K. Inoue, J. C. Harmand, T. Matsuno, High-quality $In_xGa_{1-x}As$/InAlAs

modulation-doped heterostructures grown lattice-mismatched on GaAs substrates, Journal of Crystal Growth 111 (1-4) (1991) 313–317.

[5] F. Capotondi, G. Biasiol, D. Ercolani, V. Grillo, E. Carlino, Strain induced effects on the transport properties of metamorphic InAlAs/InGaAs quantum wells, Thin Solid Films 484 (2005) 400–407.

[6] C. Heyn, S. Mendach, S. Löhr, S. Beyer, S. Schnüll, Growth of shallow InAs HEMTs with metamorphic buffer, Journal of Crystal Growth 251 (2003) 832–836.

[7] P. Ramvall, N. Carlsson, P. Omling, L. Samuelson, W. Seifert, Q. Wang, K. Ishibashi, Y. Aoyagi, Quantum transport in high mobility modulation doped $Ga_{0.25}In_{0.75}As$/InP quantum wells, Journal of Applied Physics 84 (4) (1998) 2112–2122.

[8] S. Gozu, T. Kita, Y. Sato, S. Yamada, M. Tomizawa, Characterization of high indium content metamorphic InGaAs/InAlAs modulation-doped heterostructures, Journal of Crystal Growth 227-228 (2001) 155–160.

[9] P. Chuang, S. Ho, L. W. Smith, F. Sfigakis, M. Pepper, C. Chen, J. Fan, J. P. Griffiths, I. Farrer, H. E. Beere, G. A. C. Jones, D. A. Ritchie, T. Chen, All-electric all-semiconductor spin field-effect transistors, Nature Nanotechnology 10 (2015) 35–39.

[10] A. Gold, Scattering time and single-particle relaxation time in a disordered two-dimensional electron gas, Physical Review B 38 (1988) 10798.

[11] F. Capotondi, G. Biasiol, I. Vobornik, L. Sorba, F. Giazotto, A. Cavallini, B. Fraboni, Two-dimensional electron gas formation in undoped $In_{0.75}Ga_{0.25}As/In_{0.75}Al_{0.25}As$ quantum wells, Journal of Vacuum Science & Technology B: Microelectronics and Nanometer Structures 22 (2) (2004) 702–706.

[12] P. J. Simmonds, H. E. Beere, D. A. Ritchie, S. N. Holmes, Growth-temperature optimization for low-carrier-density $In_{0.75}Ga_{0.25}As$-based high

electron mobility transistors on InP, Journal of Applied Physics 102 (8) (2007) 083518.

[13] R. P. Campion, K. W. Edmonds, L. X. Zhao, K. Y. Wang, C. T. Foxon, B. L. Gallagher, C. R. Staddon, The growth of gamnas films by molecular beam epitaxy using arsenic dimers, Journal of Crystal Growth 251 (2003) 311–316.

[14] I. Farrer, J. J. Harris, R. Thomson, D. Barlett, C. A. Taylor, D. A. Ritchie, Substrate temperature measurement using a commercial band-edge detection system, Journal of Crystal Growth 301-302 (2007) 88–92.

[15] N. Grandjean, J. Massies, Epitaxial growth of highly strained $In_xGa_{1-x}As$ on GaAs (001): the role of surface diffusion length, Journal of Crystal Growth 134 (1993) 51–61.

[16] C. Lavoie, T. Pinnington, E. Nodwell, T. Tiedje, R. S. Goldman, K. L. Kavanagh, J. L. Hutter, Relationship between surface morphology and strain relaxation during growth of InGaAs strained layers, Applied Physics Letters 67 (25) (1995) 3744.

[17] D. Ercolani, G. Biasiol, E. Cancellieri, M. Rosini, C. Jacoboni, F. Carillo, S. Heun, L. Sorba, F. Nolting, Transport anisotropy in $in_{0.75}ga_{0.25}as$ two-dimensional electron gases induced by indium concentration modulation, Physical Review B 77 (2008) 235307.

[18] P. J. Simmonds, S. N. Holmes, H. E. Beere, D. A. Ritchie, Spin-orbit coupling in an $In_{0.52}Ga_{0.48}As$ quantum well with two populated subbands, Journal of Applied Physics 103 (8) (2008) 124506.

[19] S. N. Holmes, P. J. Simmonds, H. E. Beere, F. Sfigakis, I. Farrer, D. A. Ritchie, M. Pepper, Bychkov-Rashba dominated band structure in an $In_{0.75}Ga_{0.25}/In_{0.75}Al_{0.25}$ device with spin-split carrier densities of $<10^{11}$ cm^{-2}, Journal of Physics: Condensed Matter 20 (2008) 472207.

[20] R. Winkler, Spin-Orbit Coupling Effects in Two-Dimensional Electron and Hole Systems, Springer Berlin Heidelberg, 2003.

[21] A. Gold, Electronic transport properties of a two-dimensional electron gas in a silicon quantum-well structure at low temperature, Physical Review B 35 (1987) 723.

[22] Y. Fedoryshyn, M. Beck, P. Kaspar, Characterization of Si volume-and delta-doped InGaAs grown by molecular beam epitaxy, Journal of Applied Physics 107 (2010) 093710.

[23] W. Y. Mak, K. Das Gupta, H. E. Beere, I. Farrer, F. Sfigakis, D. A. Ritchie, Distinguishing impurity concentrations in GaAs and AlGaAs using very shallow undoped heterostructures, Applied Physics Letters 97 (2010) 242107.

[24] A. Richter, M. Koch, T. Matsuyama, C. Heyn, U. Merkt, Transport properties of modulation-doped InAs-inserted-channel $In_{0.75}Al_{0.25}As/In_{0.75}Ga_{0.25}As$ structures grown on GaAs substrates, Applied Physics Letters 77 (20) (2000) 3227.